Water Research 155 (2019) 455–464

Contents lists available at ScienceDirect

Water Research

journal homepage: www.elsevier.com/locate/watres

Sustaining efficient production of aqueous iron during repeated operation of Fe(0)-electrocoagulation

Simon Müller [1], Thilo Behrends, Case M. van Genuchten*

Department of Earth Sciences, Geochemistry, Faculty of Geosciences, Utrecht University, 3584CB Utrecht, the Netherlands

ARTICLE INFO

Article history:
Received 3 October 2018
Received in revised form
20 November 2018
Accepted 21 November 2018
Available online 25 November 2018

Keywords:
Iron-electrocoagulation
Faradaic efficiency
Surface layer formation
Low cost water treatment
Charge dosage rate
Iron oxide minerals

ABSTRACT

Iron-electrocoagulation is a promising contaminant (e.g. arsenic) removal technology that is based on electrochemical Fe(II) production from steel electrodes and subsequent transport of Fe(II) to the bulk solution, where contaminant removal occurs. Although Fe-electrocoagulation systems have been shown to effectively remove contaminants in extended field trials, the efficiency of field systems can be lower than in laboratory studies. One hypothesis for this disparity is that the Faradaic efficiency of short-term laboratory experiments is higher than field systems operated over extended periods. The Faradaic efficiency is a pivotal performance indicator that we define as the measured Fe dosage normalized by the theoretical Fe dosage calculated by Faraday's law. In this work, we investigated the Faradaic efficiency in laboratory experiments for up to 35 operating cycles (>2 months) with varied Fe(0) anode purity, charge dosage rate, and electrolyte composition. Our results showed that the Faradaic efficiency decreased continuously during repeated operation under typical field conditions (charge dosage rate = 4 C/L/min, synthetic groundwater) regardless of the Fe(0) anode purity, leading to a Faradaic efficiency ≈ 0.6 after 2 months. By contrast, increasing the charge dosage rate to ≥15 C/L/min produced a Faradaic efficiency >0.85 over the entire experiment for both Fe(0) anode purities. Electrolyte solutions free of oxyanions also resulted in sustained Faradaic efficiency >0.85, regardless of the charge dosage rate. Our results confirm a previously proposed relationship between low Faradaic efficiency and the formation of macroscopic electrode surface layers, which consist of Fe (oxyhydr)oxides on the anode and a mixture of Fe (oxyhydr)oxides and calcite on the cathode. Based on these results, we discuss potential strategies to maintain a high Faradaic efficiency during Fe-electrocoagulation field treatment.

1. Introduction

Iron-electrocoagulation (Fe-EC) is a promising alternative water treatment method that is based on applying an electric current to a sacrificial Fe(0) metal anode to produce Fe(II) in solution (Lakshmanan et al., 2009): $Fe^0 \rightarrow Fe^{2+} + 2e^-$ (equation 1).

Contaminant removal in Fe-EC relies on the migration of electrochemically generated Fe(II) from the electrode to the bulk solution, where it can directly reduce contaminants, e.g. Cr(VI) (Pan et al., 2016), or be oxidized by dissolved oxygen (DO) to produce Fe coagulants that bind co-occurring solutes. Fe-EC has been shown to effectively remove a range of contaminants such as (heavy) metals and metalloids (Akbal and Camcı, 2011), oil (Chen et al., 2000), and *Escherichia coli* (Delaire et al., 2015) from different source waters. Although Fe-EC can be implemented in conventional water treatment plants, this technology has found particular application in decentralized communities (e.g. arsenic-affected regions in South Asia) because Fe-EC systems can be manufactured, operated, and maintained using only locally available materials (Amrose et al., 2013; Kumar et al., 2004). For example, extended Fe-EC field trials in West Bengal, India showed consistent removal of arsenic from local groundwater to below 5 μg/L for several months (Amrose et al., 2014). However, despite these encouraging field results, the arsenic removal efficiency of field systems operated over extended periods has been reported to be up to five times lower than laboratory systems, which are typically only operated over a limited number of cycles (Amrose et al., 2014; van Genuchten et al., 2016).

One explanation for the reported disparity in treatment efficiency relates to a decrease in the Faradaic efficiency (*FE*) of field Fe-

* Corresponding author.
E-mail address: c.m.vangenuchten@uu.nl (C.M. van Genuchten).
[1] Current address: Evides Water Company, P.O. box 4472, 3006 AL Rotterdam, the Netherlands.

https://doi.org/10.1016/j.watres.2018.11.060

Abbreviations

CDR	Charge dosage rate [C/L/min]
Fe-EC	Iron-electrocoagulation; synonyms: Fe(0)-electrocoagulation
FE	Faradaic efficiency [measured Fe concentration/theoretical Fe concentration]; synonyms: current efficiency, coulombic efficiency
IP	(Anode) interface potential [V vs Ag/AgCl]; synonyms: E_A
SGW	Synthetic groundwater
SL	Surface layer; synonyms: Oxidation layer, rust layer, oxide layer

EC systems over repeated cycles of operation, i.e. cycles of Fe-EC cell operation and overnight electrode air drying. In Fe-EC, the applied current is directly related to the concentration of Fe(II) produced by Faraday's law (equation 2): $[Fe]_{Faraday} = I \cdot t/(n \cdot F \cdot V)$,

where I represents the current (C/s) applied for an electrolysis time t (s), n represents the number of transferred electrons (2 for Fe(II) production), F represents Faraday's constant (96485 C/mol) and V represents the electrolyte volume (L). Following previous work (van Genuchten et al., 2017), we define the Faradaic efficiency (*FE*) as the total Fe concentration measured in the bulk suspension normalized by the Fe concentration predicted by Faraday's law assuming $n = 2$ in equation 2. We note that our definition encompasses two independent processes: one related to the electrochemical production of aqueous Fe, and one related to the migration of electrochemically-generated Fe from the electrode surface to the bulk solution. Based on this definition, an ideal *FE* of 1.0 indicates that all charge passed through the anode goes to Fe(II) production and transport to the bulk suspension. A $FE < 1$ indicates poor Fe(II) production and/or transport to the bulk electrolyte, resulting in a lower Fe dose per coulomb of charge passed. Since contaminant removal in Fe-EC relies on effective Fe(II) production and transport to the bulk electrolyte (Delaire et al., 2016; Kumar et al., 2004; Wan et al., 2011), a decrease in *FE* over time would decrease Fe-EC treatment performance.

Low *FE* in Fe-EC systems can originate from two principal processes (Dubrawski et al., 2015; Schultze and Lohrengel, 2000; Timmes et al., 2010): i) the applied current oxidizes Fe(0) to produce Fe(II), but the transport of Fe(II) from the electrode to the bulk is inhibited or ii) the applied current is diverted to competing electrochemical side reactions rather than Fe(0) oxidation. In the first case, a low *FE* would occur if Fe(II) is the primary product of electrochemical Fe(0) oxidation, but the generated Fe(II) deposits on the Fe(0) electrodes to form a macroscopic electrode surface layer (SL) (Timmes et al., 2010). Once formed, this SL of oxidized Fe can subsequently trap more EC-generated Fe(II), leading to SL growth over time at the expense of the *FE*. This process has been proposed previously to explain the reduced efficiency of field Fe-EC systems based on observations of extensive electrode SL formation, but has not been tested systematically in controlled experiments (Timmes et al., 2010; van Genuchten et al., 2016). In this scheme, solution conditions (i.e. pH, ionic composition) and Fe-EC operating parameters that favor SL growth would decrease the *FE* over extended operation, which would impair contaminant removal performance. One key operating parameter hypothesized to impact SL formation is the charge dosage rate (*CDR*), which is proportional to the operating current (Table S1). By increasing the *CDR*, the rate of Fe(II) addition increases, and strong chemical gradients and electric fields near the anode are produced that can alter the transport or local accumulation of Fe(II).

Poor *FE* can also occur when the applied current oxidizes redox active solutes or water instead of the Fe(0) anode (van Genuchten et al., 2017). In this case, the anodic interface potential (*IP*) is a key factor, with high *IP* favoring competing oxidation reactions. By the Butler-Volmer equation (Table S1), the anodic *IP* is directly proportional to the applied current density (Bard and Faulkner, 2001). Therefore, as shown in previous work, the *IP* during Fe-EC treatment can easily increase above 3–4 V vs Ag/AgCl at high current densities ($i > 10$ mA/cm^2), which can lead to the oxidation of H_2O to form O_2 (Dubrawski et al., 2015; van Genuchten et al., 2017). The *IP* can also be impacted by other factors, including the composition of the electrolyte solution (van Genuchten et al., 2017) and the presence of poorly conducting electrode SLs (Cornell and Schwertmann, 2003; Schultze and Lohrengel, 2000). Taken together, both causes of reduced *FE* (i.e. SL formation or competing oxidation reactions) reveal the potential importance of several factors on the long-term *FE*, and thus sustained Fe-EC system performance. However, the concomitant influence of these factors on the *FE* behavior over extended periods is unknown.

In this study, we track the *FE* and anodic *IP* of Fe-EC systems over repeated cycles of operation for up to 2 months (35 runs) as a function of the Fe(0) electrode purity, solution composition, and EC operating parameters. We focus on the release of aqueous Fe from the Fe(0) electrode, rather than the removal efficiency of any particular contaminant, since Fe(II) production is the fundamental process that underpins contaminant removal during Fe-EC treatment (Delaire et al., 2016; Kumar et al., 2004; Wan et al., 2011). Experiments were designed partly to replicate the operation of field Fe-EC systems that currently treat arsenic-contaminated groundwater in West Bengal, India, i.e. identical Fe dosage variables, electrode storage, and polarity reversal (Amrose et al., 2014). To identify the parameters that govern the *FE* over extended operation, we examined a range of applied currents, which correspond to charge dosage rates (*CDR*) from 4 to 54 C/L/min, and varied systematically the electrolyte composition. The growth of electrode SLs was measured in each experiment and the SL mineralogy was characterized by X-ray diffraction and Fe K-edge X-ray absorption spectroscopy. Our results show that a specific range of (electro) chemical conditions can sustain efficient *FE* for month timescales, which is necessary for the upscaling and widespread adoption of Fe-EC in both high- and low-income countries. Based on these results, we propose options that can be implemented by operators of Fe-EC systems in the field to ensure reliable treatment over time.

2. Methods

2.1. Electrolytes

Synthetic groundwater (SGW, composition summarized in Table 1) was prepared in 10 L batches following previous approaches, with the composition selected to best represent arsenic contaminated groundwater in South Asia, which is often targeted for treatment by Fe-EC (BGS and DPHE, 2001; Roberts et al., 2004; van Genuchten et al., 2014). Each 10 L batch of SGW was prepared by adding defined volumes of stock solutions of 0.8 M $NaHCO_3$, 0.3 M $CaCl_2$, and 0.2 M $MgCl_2 \cdot 6H_2O$ to ultrapure deionized (DI) water. Following the addition of these components, solution pH was set to 7 by conveying $CO_{2(g)}$ through the solution until the pH was reached. Under vigorous stirring, silicate was added from a freshly prepared 0.02 M stock solution ($Na_2SiO_3 \cdot 9H_2O$). Finally, phosphate was added from a 0.1 M stock solution ($Na_2HPO_4 \cdot 7H_2O$). Due to its trace concentration, arsenic was not added to the SGW recipe. After adding all components, the dissolved oxygen (DO) was decreased to 2.8–3.7 mg/L by bubbling $N_{2(g)}$ and, if needed, $CO_{2(g)}$

Table 1
Ionic composition of electrolyte solutions.

	Na^+ (mM)	Ca^{2+} (mM)	Mg^{2+} (mM)	HCO_3^- (mM)	Cl^- (mM)	HPO_4^{2-} (mM)	SiO_3^{2-} (mM)	Conductivity (μS/cm)
SGW	10.4	2.5	1.6	8.2	8.2	0.1	1	1673
Soft_SGW	18.6	0	0	8.2	8.2	0.1	1	1752
Oxyanion-free	0	2.5	1.6	0	8.2	0	0	900

A NaCl electrolyte was also used, which consisted of 10 mM NaCl.

to ensure the pH was 7. The SGW batches were stored in air-tight containers with a small head space. The DO and pH of the SGW solutions were measured with Hach LDO101 and PHC101 probes before and after each operating cycle (Table 2). The solution conductivity was measured with a Hach CDC401 probe before each experimenal series. Two types of modified SGW were prepared in 2 L batches by excluding Ca and Mg (Soft_SGW) to prevent the formation of Ca/Mg-bearing minerals during the experiments, or by excluding carbonate, silicate, and phosphate (Oxyanion-free), which have high affinities to co-precipitate with Fe oxides. We also prepared an electrolyte solution containing only 10 mM NaCl. To ensure equal chloride concentrations in all SGW variations (Table 1), NaCl was added to Soft_SGW (sodium concentrations were not equal).

2.2. Electrocoagulation experiments

2.2.1. EC cell operation

The EC cell typically consisted of two steel electrodes spaced 1 cm apart with a submerged anodic surface area of 18 cm^2 (Fig. S1). Prior to the first operating cycle, the electrodes were cleaned with concentrated hydrochloric acid, rinsed with DI water, and polished with fine grained sandpaper. No electrode cleaning occurred after the initial operating cycle. Experiments were performed in 200 mL solutions open to the atmosphere at 20 °C. The solution was stirred with a magnetic stir bar at speeds representative of the typical mixing of Fe-EC field systems (Amrose et al., 2014). Experiments were initiated by applying a constant current to the submerged electrodes using a bench top power supply (TENMA 72–10500) that was equipped with a voltmeter to measure the total cell potential. The total cell potential is an important parameter that determines the power required to pass charge during Fe-EC treatment and includes the anodic and cathodic *IP* and resistance across the aqueous solution. Standard experiments were performed using a current of roughly 14.5 mA applied for 105 min in SGW to yield 2.3 mM total Fe(II), with a current density of 0.8 mA/cm^2 and a *CDR* of 4.3 C/L/min. These operational parameters were selected to reproduce Fe-EC operating parameters used in the field and are referred to as reference experiments (Amrose et al., 2014). The *IP* was measured after 40 and 85 min of electrolysis with an Ag/AgCl reference electrode (double junction, 3 M KCl). The Fe(0) electrodes were removed after electrolysis and stored on a rack open to the atmosphere, thus ending one cycle of Fe-EC cell operation. A wide mouth pipette was used to obtain aliquots of the final suspension for measurements of total Fe following a modified SMWW protocol (APHA, 2005). These general procedures were followed for all experiments, with systematic changes in operating and chemical parameters described below.

2.2.2. Experimental conditions

The influence of Fe(0) electrode purity was evaluated by using anodes of 99% Fe by mass (Lab anodes) and anodes obtained directly from an existing Fe-EC field system installed in West Bengal, India (Field anodes, 92% Fe, composition reported previously (van Genuchten et al., 2016)). A smaller electrolyte volume was used in Field anode experiments to account for their smaller size and maintain a constant surface area to volume ratio (A/V = 90 cm^2/L). The impact of the *CDR* was investigated by systematically varying this parameter in individual experiments from 4 to 54 C/L/min. For brevity, we identify experiments with the higher and lower purity electrodes as Lab and Field, respectively, with the *CDR* indicated in the suffix (i.e. Field_54 corresponds to Field anode

Table 2
Overview of experiments: operating conditions, solution parameters and electrode properties.

Experiment Code	Anode Material	Electrolyte Solution	Charge Dosage Rate (C/L/min)	Anode Current Density[a] (mA/cm^2)	Treatment Time (min)	Initial pH	Final pH	Final DO[b] (mg/L)	Surface Layer Mass Anode (mg/cm^2)	Surface Layer Mass Cathode (mg/cm^2)
Lab_04	Lab	SGW	4.3	0.80	105	7.0 ± 0.0	7.6 ± 0.1	3.9 ± 0.9	1.8	6.6
Lab_15	Lab	SGW	15	2.8	30	7.0 ± 0.1	7.6 ± 0.2	0.1 ± 0.1	0.2	1.5
Lab_32	Lab	SGW	32	6.0	14	7.0 ± 0.1	7.6 ± 0.1	0.2 ± 0.1	0.2	0.7
Lab_54	Lab	SGW	54	10	8.4	7.0 ± 0.1	7.7 ± 0.1	0.2 ± 0.1	0.2	1.0
Field_04	Field	SGW	4.3	0.80	105	7.0 ± 0.0	7.6 ± 0.1	3.0 ± 0.9	0.6	6.8
Field_54	Field	SGW	54	10	8.4	7.0 ± 0.1	7.5 ± 0.3	0.2 ± 0.1	NA	NA
Soft_SGW	Lab	Soft_SGW	4.3	0.80	105	7.0 ± 0.1	8.3 ± 0.1	3.4 ± 0.9	1.8	0.7
Oxyanion-free	Lab	Oxyanion-free	4.3	0.80	105	6.8 ± 0.5	6.2 ± 0.3	3.3 ± 0.6	0.3	6.2
NaCl_04	Lab	NaCl	4.3	0.80	105	8.8 ± 0.7	8.5 ± 0.5	2.3 ± 0.8	1.2	1.6
NaCl_54	Lab	NaCl	54	10	8.4	8.5 ± 0.8	9.9 ± 0.1	0.2 ± 0.1	0.2	0.8
O_2_54	Lab	SGW	54	10	8.4	7.0 ± 0.1	8.1 ± 0.1	6.0 ± 0.7	0.8	1.2
Polarity-1	Lab	SGW	4.3	0.80	105	7.0 ± 0.1	7.5 ± 0.1	3.7 ± 0.8	5.8	8.6
Polarity-5	Lab	SGW	4.3	0.80	105	7.0 ± 0.1	7.8 ± 0.1	4.6 ± 0.5	10.5	9.5
SGW-storage	Lab	SGW	4.3	0.80	105	7.0 ± 0.0	7.7 ± 0.1	4.3 ± 0.8	20.2	13.7

The coulombic dose was 450 C/L for all experiments.
[a] Different surface areas were used for Lab anode (was 18 cm^2) and Field anode (9 cm^2) experiments, but the anode surface area to volume ratio (A/V = 90 cm^2/L) was maintained.
[b] The initial dissolved oxygen was 3.0 mg/L.

experiments operated at 54 C/L/min in SGW). All additional experiments described below were conducted with Lab electrodes only, which is not explicitly stated in the code.

To evaluate the impact of electrolyte composition, we performed experiments in each of the solutions described in the previous section (SGW, Soft_SGW, Oxyanion-free, NaCl). For these experiments, the *CDR* was 4 C/L/min unless otherwise noted in the suffix. In the last series of experiments, we investigated a number of previously proposed strategies to increase the long-term *FE*, including alternating the electrode polarity and varying the electrode storage conditions (Timmes et al., 2010; van Genuchten et al., 2016; Xie et al., 2017). Alternating the polarity of the electrodes, which is common practice in Fe-EC field system operation (Amrose et al., 2014) was performed in SGW once (Polarity-1) and 5 times (Polarity-5, every 21 min) per experiment. We examined the effect of drying the electrodes overnight by submerging the electrodes in SGW immediately after electrolysis (SGW-Storage) instead of air drying. An overview of the various experimental conditions and corresponding codes is given in Table 2.

2.3. Characterization of electrode surface layers

The mass of SLs formed on the anodes and cathodes was quantified by mechanically removing the SLs with a brass brush. The SL mass was measured gravimetrically and normalized by the electrode surface area. This method of SL removal was favorable compared to other techniques (e.g. abrasion with sand paper, chemical extraction) because it minimized systematic error due to removing or extracting Fe(0) from the electrode. The SLs were then ground with a mortar and pestle and characterized by X-ray diffraction (XRD) and X-ray absorption spectroscopy (XAS). Powder XRD measurements (Cu K-α radiation) were performed with a Bruker D-8 diffractometer using a rotating sample stage. Diffraction patterns were collected from 15 to 75° 2θ (0.01° step sizes) with a total data collection time of approximately 4 h per sample. Fe K-edge X-ray absorption spectra were collected for a subset of samples at the Dutch-Belgium beam line (DUBBLE, BM-26a) of the European Synchrotron Radiation Facility (Borsboom et al., 1998; Nikitenko et al., 2008). Procedures for XAS sample preparation, data collection, and data analysis are given in the Supplementary Information. In addition, an extraction method was used to measure the Fe content of the SLs by treating a solid sample aliquot in 69% nitric acid for 12 h. The Fe concentration in the extracts was measured colourimetrically (APHA, 2005).

3. Results

3.1. Temporal evolution of lab and field anode reference experiments

3.1.1. Faradaic efficiency

Fig. 1A compares the *FE* of the Lab and Field anode experiments at *CDR* = 4 C/L/min in SGW (reference conditions) for up to 35 repeated operating cycles, i.e. cycles of EC cell operation and overnight air drying. The *FE* of the Lab_04 experiment began at 0.85 and decreased continuously to 0.66 over 20 runs, with strong reproducibility between replicate experiments. Increasing the number of operating cycles from n = 20 to n = 35 over 2 months of

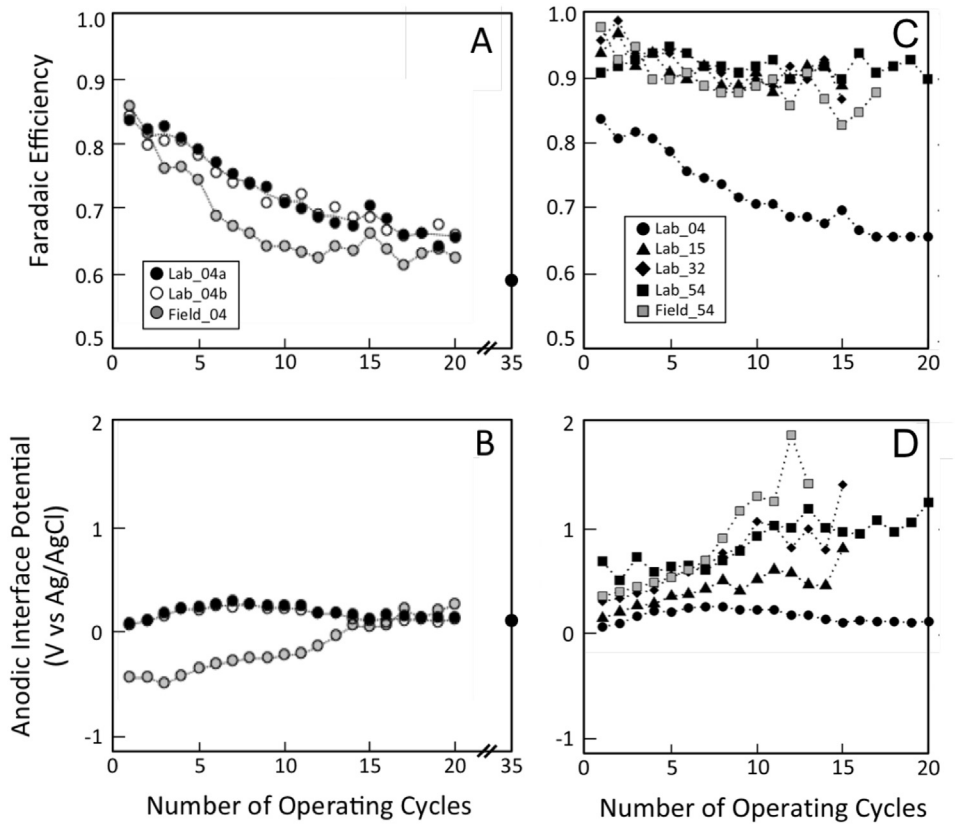

Fig. 1. Faradaic efficiency (top panels) and anodic interface potential (bottom panels) as a function of the number of operating cycles for the reference Lab_04 and Field_04 experiments (left panels) and the *CDR* experiments (right panels). In A and C, the Lab_04a and Lab_04b experiments (black filled circles and open circles) were performed in duplicate. The *FE* and the interface potential of Lab_04a after 35 runs are shown after the break in the x-axis. In C), Lab electrodes were used in all experiments except Field_54. All experiments were performed in SGW.

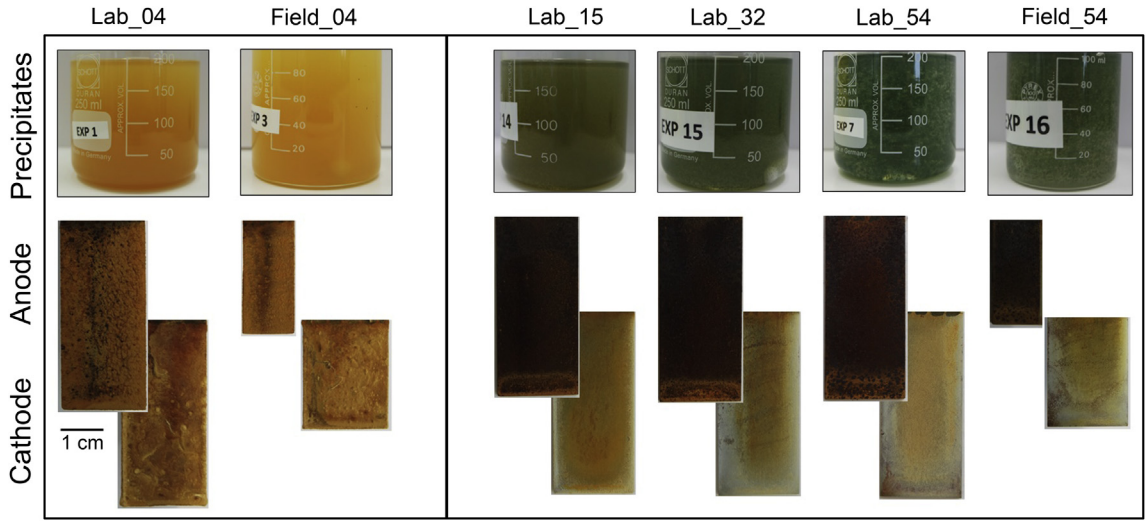

Fig. 2. Macroscopic images of the precipitates and surface layers formed on the anodes and cathodes of the Lab and Field electrodes at the end of low (left panel) and high *CDR* (right panel) experiments. All experiments were performed in SGW.

operation, which is the longest continuous experiment in this study, decreased the *FE* of the Lab_04 experiment to 0.6 (only the final data point is shown in Fig. 1). The behavior of the *FE* for the Field_04 experiment was similar to that of the Lab_04 experiment, showing an initial *FE* near 0.85 and a continuous decrease to 0.62 over 20 operating cycles. The match between the *FE* of the Lab_04 and Field_04 experiments indicates that the Fe(0) anode purity does not play a critical role in determining the *FE* at *CDR* = 4 C/L/min.

3.1.2. Anode interface potential

The behavior of the *IP* over extended operation for the Lab_04 and Field_04 experiments is shown in Fig. 1B. The *IP* of the Lab_04 experiment increased from approximately 0 V vs Ag/AgCl in the first run to 0.2 V vs Ag/AgCl after 10 runs. Despite a continuous decrease in *FE* from operating cycle 10 to 35, the *IP* of the Lab_04 experiment remained stable at 0.2 V vs Ag/AgCl. Although the Lab_04 and Field_04 experiments showed nearly identical *FE* over time, slight differences in the *IP* of these experiments was observed. The Field_04 experiment had a lower initial *IP* (−0.4 V vs Ag/AgCl) than the Lab anode, but the *IP* of the Field_04 experiment increased almost linearly over 20 runs, resulting in a slightly higher final *IP* (0.3 V vs Ag/AgCl) than in the Lab_04 experiment. The total cell voltage of the Field_04 experiment also increased slightly over time from 1.4 V to 2.4 V, whereas the Lab_04 experiment was stable at 2.3 V.

3.1.3. Surface layer formation

Fig. 2 shows visually the macroscopic electrode SLs formed after 35 operating cycles in the reference experiments (Fig. S2 presents a detailed time-series). The onset of a SL occurred on the Lab_04 anode after the first run, and by operating cycle 8, the SL completely covered the Fe(0) surface. Over 35 runs, the texture of this SL became rough and the colour changed from yellow to dark orange. Macroscopic anodic SLs were also observed in Field_04 experiments (Fig. 2). Slightly more SL was produced in the Lab anode (1.8 mg/cm^2) experiment relative to the Field anode (0.6 mg/cm^2, Table 2). X-ray diffraction revealed that the anodic SLs for both Lab_04 and Field_04 experiments consisted of ferrihydrite-like, poorly ordered Fe(III) precipitates based on the broad peak near 35° 2θ (Fig. 3). The line shape and positions of major oscillations in the Fe K-edge EXAFS spectrum (Fig. S3) of the Lab_04 anodic SLs are consistent with oxyanion-rich, disordered Fe(III) precipitates with less Fe—Fe polymerization than 2-line ferrihydrite. No features in the X-ray diffractograms of the anodic SLs of the Lab_04 and Field_04 experiments were consistent with goethite, lepidocrocite, or other Fe(II,III) minerals common in corrosion layers (Cook, 2005; Cornell and Schwertmann, 2003). The presence of poorly crystalline Fe(III) precipitates in the SLs is likely due to the composition of the SGW electrolyte, which contains high concentrations of

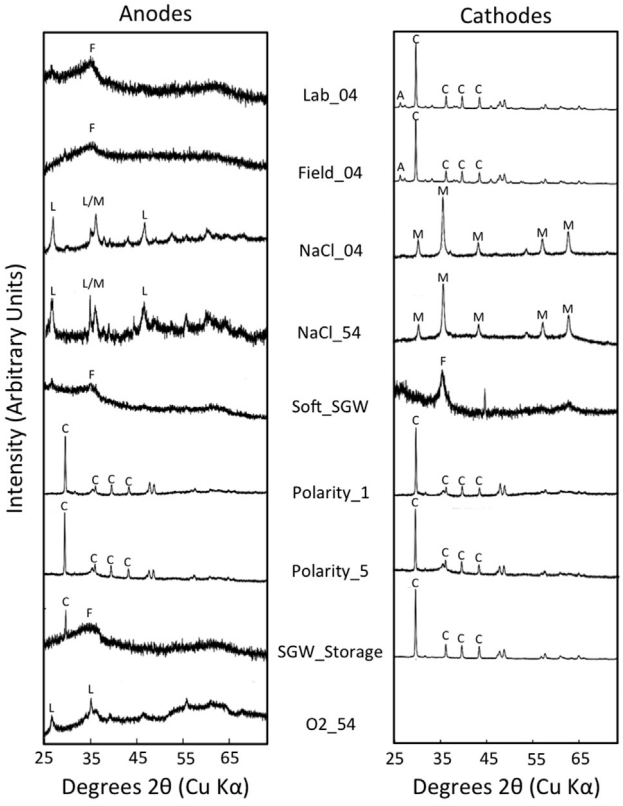

Fig. 3. Powder X-ray diffractograms of surface layers formed during selected experiments. The major peaks arising from lepidocrocite, magnetite, ferrihydrite, calcite, and aragonite are indicated by L, M, F, C, and A, respectively.

surface-poisoning silicate and phosphate (Senn et al., 2015; Voegelin et al., 2013).

The formation and growth of cathodic SLs were also observed in the Lab_04 and Field_04 experiments, but the properties of these SLs were different than the anodic SLs. For both cathodes, orange SLs formed after 3–7 runs, and after 20–35 runs, the cathodic SLs became darker and more heterogeneous, with clear white spots (Fig. 2). In contrast to the anodic SLs, the cathodic SLs were brittle, cracked, and did not adhere strongly to the electrode. Nearly identical SL quantities formed on the Lab_04 (6.6 mg/cm^2) and Field_04 (6.8 mg/cm^2) cathodes, which is consistent with their similar colour and texture (Table 2). In contrast to the X-ray diffractograms of the anodic SLs, diffraction peaks from $CaCO_3$ were the dominant features of the X-ray diffractograms of the cathodic SLs (Fig. 3). While no evidence for crystalline Fe mineral phases appeared in the X-ray diffractograms of the cathodic SLs, the brownish SL colour and the detection of Fe in HNO_3-digested samples by wet chemical methods suggests that the SLs contained Fe(III) precipitates. The Fe K-edge XANES and EXAFS spectrum of the Lab_04 cathodic SL (Fig. S3) confirmed the presence of disordered Fe(III) precipitates, which were also present in the Lab_04 anodic SL. The presence of a greater fraction of $CaCO_3$ in the cathodic SLs is consistent with the larger masses of these SLs relative to the anodic SLs and suggests that different processes contribute to anodic and cathodic SL formation.

3.2. Impact of charge dosage rate

3.2.1. Faradaic efficiency

Fig. 1C shows the *FE* for Lab and Field anode experiments performed at different *CDR* values over 15 to 20 operating cycles in SGW. The *FE* was highly dependent on the *CDR* using Lab anodes, with increasing *CDR* favoring increased and sustained *FE*. At *CDR* $\geq$ 15 C/L/min, the *FE* for the Lab anodes on the first run was between 0.9 and 1.0, which is higher than the 0.85 FE of the first cycle of the reference experiments at *CDR* of 4 C/L/min. The first run of the experiment using the Field anode at increased *CDR* (54 C/L/min) also showed a high *FE* above 0.95 (Fig. 1). Remarkably, the *FE* at *CDR* $\geq$ 15 C/L/min remained above 0.85 throughout the entire 15 to 20 runs in both Lab and Field anode experiments, which contrasts the continuous *FE* decrease in experiments at low *CDR*. Experiments performed at *CDR* of 15, 32, and 54 C/L/min all yielded similarly high and sustained *FE*, which suggests a threshold *CDR* exists between 4 and 15 C/L/min that sustains high *FE*.

3.2.2. Anode interface potential

The effect of *CDR* on the *IP* is shown in Fig. 1D. The *IP* of the initial runs for both Lab and Field anodes increased with increasing *CDR*, which is consistent with the Butler-Volmer relationship (Bard and Faulkner, 2001). In contrast to the stable *IP* of the low *CDR* experiments, the *IP* of experiments at elevated *CDR* increased with the number of operating cycles. This trend in *IP* was most pronounced for the Field_54 experiment, which was below 0.5 V vs Ag/AgCl initially, but exceeded 2 V vs Ag/AgCl after 15 runs. Despite *IP* values above 2 V vs Ag/AgCl, a *FE* > 0.85 was maintained in these experiments, indicating the production of Fe(II) was the dominant reaction on the anode. Consistent with the *IP* measurements, the total cell voltage of all experiments increased over repeated operation, with the largest increase from 7 to 11 V observed in the Field_54 experiment after 16 runs.

3.2.3. Surface layer formation

The macroscopic properties of the electrode SLs depended strongly on the *CDR* (Fig. 2, Fig. S4). For experiments at *CDR* $\geq$ 15 C/L/min, only small quantities of anodic SLs were produced (0.2 mg/cm^2) and these were darker compared to experiments at low *CDR*. On the cathodes, a very bright SL developed (orange at the electrode center, white near the edge) and none of the macroscopic cracks found in the cathodic SLs for low *CDR* experiments were observed. In addition, the quantity of cathodic SLs at *CDR* > 15 C/L/min (0.7–1.5 mg/cm^2, Table 2) was substantially smaller than the low *CDR* experiments (>6 mg/cm^2).

3.3. Electrolyte composition effects

3.3.1. Faradaic efficiency

The composition of the electrolyte played a critical role in the behavior of the *FE* over extended operating cycles (Fig. 4A). Regardless of the low *CDR*, a stable *FE* > 0.9 was observed for all runs in electrolytes containing no oxyanions, such as the oxyanion-free SGW electrolyte (Oxyanion-free) and the NaCl electrolyte. When oxyanions (P, Si, and inorganic carbon) were present, the decrease in *FE* over extended operating cycles was similar in the presence and absence of Ca and Mg. For example, the *FE* in the Soft_SGW electrolyte over 15 operating cycles closely resembled the reference experiments in SGW, beginning near 0.85 and decreasing to below 0.7. The observations of sustained *FE* over repeated operating cycles in SGW at high *CDR* and in Oxyanion-free SGW at low *CDR* indicates that maintaining high *FE* depends on both the electrolyte composition and the *CDR*. Because the *FE* was already above 0.9 for the NaCl_04 experiment, increasing the *CDR* in this electrolyte did not further increase the *FE*.

3.3.2. Anode interface potential

A considerably lower *IP* was observed in the absence of oxyanions (Fig. 4B), with the Oxyanion-free and NaCl experiments remaining near −0.4 to −0.3 V vs Ag/AgCl over the entire experimental duration. Consistent with the behavior of the *FE* in the Soft_SGW experiment, the presence or absence of bivalent cations (Ca and Mg) did not impact the *IP*. In agreement with the high *CDR* experiments in SGW, increasing *CDR* from 4 to 54 C/L/min also increased the initial *IP* in the NaCl electrolyte from −0.4 to 0.7 V vs Ag/AgCl. However, the same continued increase in *IP* over 20 runs observed in SGW was not observed in the NaCl electrolyte.

3.3.3. Surface layer formation

The composition of the electrolyte altered the formation and growth of SLs on both anodes and cathodes. In the Oxyanion-free experiments, where a high *FE* was sustained, only 0.3 mg/cm^2 of dark reddish SL was produced on the anode during the experiment (Fig. S5, Table 2). By contrast, 1.8 mg/cm^2 was removed from the anode used in the Soft_SGW experiments, which was the same anodic SL amount in the analogous SGW experiment. The anodic SLs for the Soft_SGW experiment consisted of primarily poorly-crystalline Fe(III) precipitates, which was also observed in the reference experiments (Fig. 3). Approximately 1.2 and 0.2 mg/cm^2 were removed from the anodes in the NaCl_04 and NaCl_54 experiments and lepidocrocite was the major phase detected by XRD in these SLs (Fig. 3).

The amount of cathodic SLs that formed in the Oxyanion-free experiment (6.2 mg/cm^2) matched that of the analogous SGW experiment (6.6 mg/cm^2). In the Soft_SGW electrolyte, which contained no bivalent cations and prevented $CaCO_3$ formation, bare metal was still observed on the cathode after the entire experimental duration (15 operating cycles) and only 0.7 mg/cm^2 was removed (Table 2). The cathodic SLs generated in the Soft_SGW electrolyte were found to consist of primarily poorly-crystalline Fe(III) precipitates based on XRD (Fig. 3). Black SLs displaying magnetite peaks in XRD formed on the cathodes in NaCl_04 and NaCl_54 experiments, with greater SL mass formed in the NaCl_04

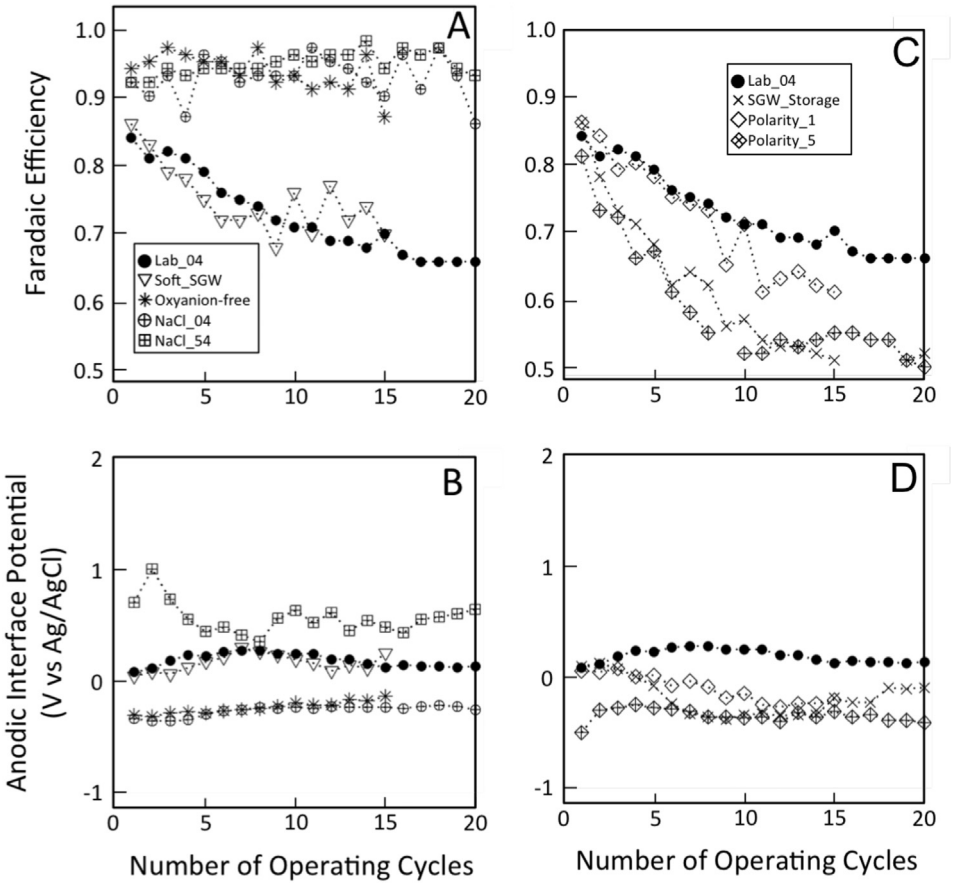

Fig. 4. Faradaic efficiency (top panels) and anodic interface potential (bottom panels) as a function of the number of operating cycles for experiments performed in electrolytes of different composition (left panels) and with different polarity reversal and electrode storage conditions (right panels). Experiments shown in the right panels were performed in SGW.

experiment (1.6 mg/cm^2) relative to NaCl_54 (0.8 mg/cm^2).

3.4. Polarization alteration and electrode storage

3.4.1. Faradaic efficiency

Fig. 4C shows that single polarity reversal (Polarity_1) between every operating cycle decreased the *FE* similar to the experiments without polarity reversal (the Lab_04 reference experiments) until run number 10. After run 10, the *FE* of Polarity_1 experiments was consistently lower than experiments without polarity reversal. Reversing the polarity 5 times during each operating cycle resulted in a more rapid decrease in *FE* to below 0.5 after only 10 runs. Overnight electrode storage in SGW was also unsuccessful at sustaining *FE* over extended operating cycles. Fig. 4C shows that the *FE* of SGW_Storage experiments decreased more rapidly than for dry storage conditions, reaching 0.5 after 20 runs.

3.4.2. Anode interface potential

Although the polarity alteration experiments did not sustain the *FE*, these experiments did produce a lower *IP* over extended operation (Fig. 4D), with a final *IP* for the Polarity_1 and Polarity_5 experiments near −0.3 V vs Ag/AgCl. The total cell voltages of these experiments were also the lowest in our study and decreased with increasing operating cycles (Table S2). The *IP* of the SGW_Storage experiments was slightly lower than dry storage conditions and ended at −0.2 V vs Ag/AgCl after 20 runs.

3.4.3. Surface layer formation

Reversing the electrode polarity strongly impacted properties of the electrode SLs. The Polarity_1 and Polarity_5 electrodes displayed a brittle orange layer that chipped away from the electrode easily, which is similar to the cathodic SLs formed in other experiments. These results are consistent with both electrodes serving as anode and cathode. Large SL quantities formed on these electrodes (7.2 mg/cm^2 for Polarity_1 and 10 mg/cm^2 for Polarity_5, Table 2). The X-ray diffractograms of the Polartiy-1 and Polarity_5 SLs indicated the presence of $CaCO_3$ (Fig. 3), while the Fe K-edge EXAFS spectrum of the Polarity_1 SLs indicated the presence of poorly-crystalline Fe(III) precipitates with similar structure to the solids contained in the reference Lab_04 anodic SL (Fig. S3). The SGW_Storage electrodes produced the largest quantity of anodic SLs (20 mg/cm^2) and both anodic and cathodic SLs consisted of a mixture of $CaCO_3$ and poorly-crystalline Fe(III) precipitates.

4. Discussion

4.1. Repeated operation decreases FE in conditions representative of Fe-EC field treatment

The results for Fe-EC experiments with operating parameters and solution composition representative of Fe-EC field treatment support the hypothesis that operating Fe-EC under field conditions can lead to a decrease in *FE*, which adversely effects Fe-EC performance. The Lab_04, Field_04, and Polarity_1 experiments replicate closely the raw water composition and operating conditions (i.e.

CDR, electrolysis time, current density, A/V ratio, dry storage) used in existing Fe-EC plants that treat arsenic-contaminated groundwater (van Genuchten et al., 2016). Our results showed a systematic decrease in the *FE* with repeated operation in each of these experiments. For example, the *FE* continuously decreased over the two-month long duration of the Lab_04 experiment, leading to a 40% lower Fe dose to solution than expected by Faraday's law. This decrease in *FE* would impair contaminant removal efficiency by decreasing the amount of Fe available to sorb or reduce the target species for a given coulomb of charge passed. A decrease in *FE* over extended operation was also observed in the Field_04 and Polarity_1 experiments, which replicate even closer Fe-EC field treatment (Field_04 uses a lower purity anode taken from an existing Fe-EC plant in India; Polarity_1 applies the same cycle of polarity reversal). Therefore, our results confirm a previous hypothesis that a decrease in *FE* contributes to the poorer contaminant removal efficiency observed for Fe-EC electrodes with a large SL build-up relative to newly-cleaned and well-maintained Fe-EC electrodes (van Genuchten et al., 2016). This conclusion is consistent with the similar growth of Fe-bearing anodic SLs in the Lab_04, Field_04, and Polarity_1 experiments and the SLs documented in Fe-EC field systems operated for many months.

4.2. Electrochemical and solution chemical variables that sustain high FE

Although the experiments designed to mimic existing Fe-EC plant operation showed a decreased *FE* over time, our results revealed at least two (electro)chemical variables that could be manipulated to sustain high *FE* for > 1–2 months: i) the charge dosage rate (*CDR*), and ii) the electrolyte composition. Furthermore, we observed that a sustained *FE* in these experiments correlated with low anodic SL growth. In the following sections, we discuss and provide explanations for the impact of *CDR* and electrolyte composition on the *FE* and electrode SLs.

4.2.1. Charge dosage rate

As shown in Fig. 1C, experiments at $CDR \geq 15$ C/L/min produced a larger initial *FE* (>0.9) compared to $CDR = 4$ C/L/min (<0.85), and more importantly, sustained this high *FE* over repeated operating cycles. Simultaneously, experiments at high *CDR* showed a decrease in anodic SL mass. The beneficial effect of increasing *CDR* on the *FE* can be explained by processes related to the accumulation of Fe oxides at the electrode surface. In EC systems, the *CDR* is directly proportional to the addition rate of Fe(II) (speciated as the free Fe^{2+} ion at circumneutral pH). Therefore, an increase in *CDR* from 4 to ≥15 C/L/min increases the flux of positively charged Fe^{2+} at least ≈ 4-fold, while simultaneously increasing the anodic *IP* (Fig. 1D). The combination of a higher flux of positively charged Fe^{2+} and higher positive charge of the anode increases cation diffusion and electrostatic repulsive forces between the anode and cations, which facilitates the migration of the Fe^{2+} to the bulk solution, rather than accumulation at the anode surface. Furthermore, the increased flux of Fe(II) at high *CDR* would also lead to strong chemical gradients near the anode surface, especially with respect to dissolved oxygen (DO). For example, experiments at $CDR \geq 15$ C/L/min consumed the dissolved oxygen concentration to <0.1 mg/L, which resulted in the formation of mixed-valent Fe oxides (green rust in SGW, magnetite in NaCl, see Figs. S4 and S5). This dissolved oxygen behavior contrasts that of the low *CDR* experiments, where dissolved oxygen remained near 3.0 mg/L and purely Fe(III) (oxyhydr)oxides formed. An increase in Fe(II) flux at high *CDR* can deplete dissolved oxygen levels near the anode rapidly, which would prevent Fe(II) oxidation and the formation of Fe(III)-bearing solids that can deposit on the electrode as a SL. Finally, the different macroscopic properties of the mixed-valent Fe oxides that formed in high *CDR* experiments (Fig. S4), which consisted of much larger flocs than the low *CDR* solids, could also facilitate lower SL growth and sustained *FE*. To elucidate the contribution of dissolved oxygen depletion to the increase in *FE* with increasing *CDR*, we performed a series of experiments at $CDR = 54$ C/L/min in SGW while bubbling air continuously during operation (O_2_54). In these experiments, the dissolved oxygen never decreased below 3.0 mg/L and Fe(III) precipitates formed (Fig. S4), but the *FE* still remained > 0.8 for the entire duration (15 cycles). Therefore, we expect the role of dissolved oxygen on the *FE* to be a second-order effect relative to the *CDR*.

4.2.2. Electrolyte composition

The most significant effect of electrolyte composition on the *FE* was observed in the presence of oxyanions. While changes in pH can impact many processes during Fe-EC treatment, our results indicate that pH was a secondary effect relative to the presence of oxyanions in our experiments (Table 2 summarizes the pH behavior for each experiment). As shown in Fig. 4A, the *FE* in experiments with electrolyte solutions rich in phosphate (P), silicate (Si), and carbonate (i.e. SGW and Soft_SGW) decreased over repeated operating cycles for experiments at $CDR = 4$ C/L/min. By contrast, the *FE* in electrolyte solutions free of P, Si, and carbonate (Oxyanion-free, NaCl) remained high throughout the experiment and SL growth was minimal, regardless of pH. The impact of oxyanions on the *FE* and SL properties can be attributed to two processes. First, oxyanions such as P and Si are well known to passivate Fe(0) metal in natural corrosion systems (Bojinov et al., 1999). Because of their high sorption affinity for Fe precipitates (Roberts et al., 2004), Si and P can bind to oxidized Fe at the anode surface, leading to an oxyanion-rich SL that modifies anodic properties, including decreased electrical conductance. Indeed, the presence of P in single-solute electrolytes was shown to decrease dramatically the *FE* of Fe-EC systems over single operating cycles, which was explained by the formation of passifying P-rich SLs that increased the *IP* and promoted the anodic H_2O oxidation to form O_2, rather than anodic Fe(0) oxidation (van Genuchten et al., 2017). Second, the presence of high concentrations of P and Si during the formation of Fe(III) (oxyhydr)oxides inhibits Fe(III) polymerization and leads to poorly-ordered, nanoscale particles that do not aggregate, flocculate, and settle on practical time scales (van Genuchten et al., 2014). The X-ray diffractograms (Fig. 3) and Fe K-edge EXAFS spectra (Fig. S3) of SLs in oxyanion-rich experiments confirmed the presence of poorly-crystalline Fe(III) precipitates with structures consistent with oxyanion-rich hydrous ferric oxide (Doelsch et al., 2000). It was also observed visually that the Fe(III) precipitates produced in experiments with oxyanion-rich solutions remained suspended throughout electrolysis, whereas large coagulated flocs formed readily in oxyanion-free solutions even during rapid mixing (Fig. S5 compares the visible flocs in the NaCl_04 experiment with the more colloidally stable Lab_04 suspension). Since the nanoscale, less aggregated Fe(III) precipitates formed in oxyanion-rich solutions remain in suspension longer, these solids are more likely to contact, deposit, and be trapped on the Fe(0) anode, which would decrease the *FE*.

Although the presence or absence of bivalent cations did not play a major role in altering the behavior of the *FE*, Ca and Mg were found to impact electrode SL properties in many experiments. The X-ray diffractograms of cathodic SLs were dominated by $CaCO_3$ when bivalent cations co-occurred with carbonate. This result can be explained by the combination of the negative electrode potential at the cathode, which would attract positively charged Ca and Mg cations, and the cathodic reduction of H_2O to form $H_{2(g)}$, which is the dominant cathodic reaction in Fe-EC treatment (Lakshmanan

et al., 2009). The cathodic formation of $H_{2(g)}$ consumes H^+ ions, leading to a region of high pH near the cathode, which favors the formation of carbonate minerals (e.g. $CaCO_3$, $MgCO_3$). Although we found that reactions at the anode were not affected by cathodic $CaCO_3$ formation in fixed polarity experiments, the Polarity_1 and Polarity_5 experiments displayed a lower *FE* and greater SL mass relative to the Lab_04 and Field_04 experiments. The poorer *FE* in the polarity reversal experiments can be explained by the large and porous $CaCO_3$-bearing SLs acting as sink for EC-generated Fe(II) when the cathode becomes the anode, thus inhibiting transport of aqueous Fe to the bulk solution and decreasing the *FE*. The X-ray diffractograms of SL samples from the polarity reversal experiments are dominated by $CaCO_3$, but Fe K-edge EXAFS spectroscopy (Fig. S3) confirmed that the Polarity_1 SLs contain poorly-ordered Fe(III) precipitates with structures similar to those in the Lab_04 anodic SLs.

4.3. Implications for Fe-EC field operation

This study provides a number of useful results to inform Fe-EC field treatment, including the selection of electrode materials and optimization of operational parameters and maintenance. For example, the purity of the Fe(0) anode did not significantly impact the long-term performance of the electrodes, with the Lab_04 and Field_04 experiments displaying nearly identical *FE* behavior, SL growth and mineralogy, and total cell potential. Since the impurity content of the Lab and Field electrodes varied strongly (Lab electrodes = 99% Fe, Field electrodes = 92% Fe), the similar decrease in the *FE* for these electrodes suggests that the oxidation of non-ferrous steel components, such as manganese or carbon, is not the primary driver of reduced *FE*. More importantly, these results indicate that the electrode purity is not a critical factor in Fe-EC system performance, which suggests that less costly and locally available electrode materials with lower purity can be implemented in Fe-EC field systems without sacrificing long-term efficiency. However, we note that some steel can contain toxic metal impurities (e.g. Cr, V, Ni, Sb), the release of which must be avoided during Fe(0) EC treatment. In addition, the *IP* and total cell voltage increased over extended operating cycles more for the Field anode, suggesting that higher purity steel should be used to decrease power consumption if available at similar costs as impure steel.

With respect to maintaining a stable and high *FE* over extended operation, which is critical for efficient and reliable Fe-EC field treatment, our study suggests that increasing the *CDR* and avoiding the presence of oxyanions can help to sustain the *FE*. Modifying the electrolyte composition of the untreated (raw) water to eliminate oxyanions prior to treatment is impractical at large scales, but could be done by employing a separate Fe(0) electrolysis dosing chamber with controlled solution composition that feeds into the contaminated water influent. A much more appropriate option to sustain *FE* over extended operation is to simply increase the *CDR*. This strategy requires only increasing the operating current, which can be performed easily at existing Fe-EC plants without new infrastructure. Although increasing the *CDR* decreases the total electrolysis time, which can be advantageous in areas with intermittent power supply, increasing the *CDR* also increases power consumption (0.26 kWh/m^3 at 4 C/L/min, 1.17 kWh/m^3 at 54 C/L/min, Table S2) because of the larger cell voltage and total electric work required to pass the same amount of charge. Therefore, our results suggest an optimum *CDR* exists that sustains the *FE* and minimizes power consumption, which can be identified precisely with local water using 15 C/L/min as a recommended starting value. Another consequence of increasing the *CDR* can be the formation of particles with different properties (i.e. mixed valent Fe oxides rather than Fe(III) precipitates). The impact of generating precipitates that contain structural Fe(II) (e.g. magnetite, green rust) on contaminant removal by Fe-EC could be positive or negative, but if negative, this process can be counteracted by incorporating an air-cathode into treatment design. The H_2O_2 generated by an air-cathode system would oxidize Fe(II) rapidly and prevent the accumulation of Fe(II) needed for mixed valent Fe oxide formation (Si et al., 2017).

Preventing the formation and growth of electrode SLs is another viable option to enhance the performance of Fe-EC field treatment. In this study, we investigated two low-cost methods of inhibiting SL formation that can be applied easily in existing Fe-EC treatment plants. To minimize SL growth arising from Fe(0) oxidation by atmospheric O_2 during overnight air storage, we stored the electrodes in the SGW solution between operating cycles. This strategy was not effective, resulting in greater SL growth compared to overnight air drying and one of the poorest *FE*. We also examined different cycles of polarity reversal during treatment, which is often proposed as an electrochemical method of cleaning the electrodes by cathodic reduction of Fe(III)-bearing SLs (Timmes et al., 2010). This strategy also proved unsuccessful at decreasing SL growth and maintaining high *FE*. The ineffectiveness of reversing the electrode polarity can be explained by the formation of $CaCO_3$ on the cathode, which can trap electrochemically-generated Fe(II) when the cathode becomes the anode. Since both unobtrusive methods of electrode cleaning were ineffective, physical or chemical cleaning of the electrodes can be pursued. The simplicity and reliability of SL removal by mechanical brushing fits the constraints of decentralized Fe-EC treatment and is currently practiced in some existing systems (Amrose et al., 2014), but this technique requires a large workforce. Chemical removal of SLs by strong mineral acids is effective, but requires skilled labor and proper disposal of strong acid waste. Therefore, the use of citric acid or other non-hazardous organic acids, which is often applied in potable water treatment to remove inorganic layers from filter membranes, could be a more practical option for chemical SL removal (Strugholtz et al., 2005).

5. Conclusions

The contaminant removal efficiency of Fe-EC systems hinges on the efficient anodic production of aqueous Fe(II) and transport to the bulk solution. We found a continuous decrease in *FE* to roughly 0.6, which was accompanied by electrode SL growth, over repeated operating cycles (2 months) in experiments that mimicked Fe-EC field treatment. This result helps explain reported differences in contaminant removal efficiency for lab and field Fe-EC treatment and should be considered for accurate predictions of Fe-EC treatment efficiency over extended periods. The decrease in *FE* was not related to the purity of the ≈99 and ≈ 92% Fe electrodes used in this work. Rather, the behavior of the *FE*, and the formation and growth of electrode SLs, depended more on the electrolyte composition (i.e. presence of oxyanions) and the *CDR*. Because adjusting the *CDR* in existing Fe-EC plants is simple, low-cost, and requires no new infrastructure, we propose that increasing the *CDR* is the most ideal method of sustaining the *FE* over extended operation. However, prior to adjusting the *CDR*, preliminary experiments should be performed at existing Fe-EC facilities to verify that undesirable changes to Fe oxide particle formation do not occur. Previously proposed strategies to remove SLs formed in cases of poor *FE* were unsuccessful (polarity reversal, water-saturated electrode storage), suggesting that mechanical or chemical methods could be pursued for periodic SL removal. The results of this work help inform the design of new Fe-EC systems that can achieve sustained *FE* with minimal maintenance.

Acknowledgements

We gratefully acknowledge funding provided by a NWO Veni Grant (Project No. 14400) awarded to CMvG. We would like to thank Peter Kraal, Alwina Hoving and Helen King for their support in the laboratory. We acknowledge the European Synchrotron Radiation Facility for provision of synchrotron radiation facilities and we would like to thank Dipanjan Banerjee for assistance at the Dutch-Belgium beamline (BM-26a).

Appendix A. Supplementary data

Supplementary data to this article can be found online at https://doi.org/10.1016/j.watres.2018.11.060.

References

Akbal, F., Camcı, S., 2011. Copper, chromium and nickel removal from metal plating wastewater by electrocoagulation. Desalination 269 (1), 214–222.
Amrose, S., Gadgil, A., Srinivasan, V., Kowolik, K., Muller, M., Huang, J., Kostecki, R., 2013. Arsenic removal from groundwater using iron electrocoagulation: effect of charge dosage rate. Journal of Environmental Science and Health Part A 48 (9), 1019–1030.
Amrose, S.E., Bandaru, S.R.S., Delaire, C., van Genuchten, C.M., Dutta, A., DebSarkar, A., Orr, C., Roy, J., Das, A., Gadgil, A.J., 2014. Electro-chemical arsenic remediation: field trials in West Bengal. Sci. Total Environ. 488–489, 539–546.
APHA, 2005. Standard Methods for the Examination of Water & Wastewater. American Public Health Association (APHA), Washington, DC, USA.
Bard, A.J., Faulkner, L.R., 2001. Electrochemical Methods: Fundamentals and Applications. John Wiley & Sons.
BGS and DPHE, 2001. In: Kinniburgh, D.G., Smedley, P.L. (Eds.), Arsenic Contamination of Groundwater in Bangladesh. British Geological Survey, Keyworth.
Bojinov, M., Betova, I., Fabricius, G., Laitinen, T., Raicheff, R., 1999. Passivation mechanism of iron in concentrated phosphoric acid. J. Electroanal. Chem. 475 (1), 58–65.
Borsboom, M., Bras, W., Cerjak, I., Detollenaere, D., van Loon, D., Goedtkindt, P., Konijnenburg, M., Lassing, P., Levine, Y., Munneke, B., Oversluizen, M., van Tol, R., Vlieg, E., 1998. The Dutch-Belgian beamline at the ESRF. J. Synchrotron Radiat. 5, 518–520.
Chen, X., Chen, G., Yue, P.L., 2000. Separation of pollutants from restaurant wastewater by electrocoagulation. Separ. Purif. Technol. 19 (1), 65–76.
Cook, D.C., 2005. Spectroscopic identification of protective and non-protective corrosion coatings on steel structures in marine environments. Corrosion Sci. 47 (10), 2550–2570.
Cornell, R.M., Schwertmann, U., 2003. The Iron Oxides: Structure, Properties, Reactions, Occurrences and Uses. John Wiley & Sons.
Delaire, C., van Genuchten, C., Amrose, S., Gadgil, A., 2016. Bacteria attenuation by iron electrocoagulation governed by interactions between bacterial phosphate groups and Fe(III) precipitates. Water Res. 103, 74–82.
Delaire, C., van Genuchten, C.M., Nelson, K.L., Amrose, S.E., Gadgil, A.J., 2015. Escherichia coli attenuation by Fe electrocoagulation in synthetic Bengal groundwater: effect of pH and natural organic matter. Environ. Sci. Technol. 49 (16), 9945–9953.
Doelsch, E., Rose, J., Masion, A., Bottero, J.Y., Nahon, D., Bertsch, P.M., 2000. Speciation and crystal chemistry of iron(III) chloride hydrolyzed in the presence of SiO4 ligands. 1. An FeK-edge EXAFS study. Langmuir 16 (10), 4726–4731.
Dubrawski, K.L., van Genuchten, C.M., Delaire, C., Amrose, S.E., Gadgil, A.J., Mohseni, M., 2015. Production and transformation of mixed-valent nanoparticles generated by Fe(0) electrocoagulation. Environ. Sci. Technol. 49 (4), 2171–2179.
Kumar, P.R., Chaudhari, S., Khilar, K.C., Mahajan, S.P., 2004. Removal of arsenic from water by electrocoagulation. Chemosphere 55 (9), 1245–1252.
Lakshmanan, D., Clifford, D.A., Samanta, G., 2009. Ferrous and ferric ion generation during iron electrocoagulation. Environ. Sci. Technol. 43 (10), 3853–3859.
Nikitenko, S., Beale, A., van der Eerden, A., Jacques, S., Leynaud, O., O'Brien, M., Detollenaere, D., Kaptein, R., Weckhuysen, B., Bras, W., 2008. Implementation of a combined SAXS/WAXS/QEXAFS set-up for time-resolved in situ experiments. J. Synchrotron Radiat. 15, 632–640.
Pan, C., Troyer, L., Catalano, J., Giammar, D., 2016. Dynamics of chromium(VI) removal from drinking water by iron electrocoagulation. Environ. Sci. Technol. 50 (24), 13502–13510.
Roberts, L.C., Hug, S.J., Ruettimann, T., Billah, M.M., Khan, A.W., Rahman, M.T., 2004. Arsenic removal with iron(II) and iron(III) in waters with high silicate and phosphate concentrations. Environ. Sci. Technol. 38 (1), 307–315.
Schultze, J.W., Lohrengel, M., 2000. Stability, reactivity and breakdown of passive films. Problems of recent and future research. Electrochim. Acta 45 (15), 2499–2513.
Senn, A., Kaegi, R., Hug, S., Hering, J., Mangold, S., Voegelin, A., 2015. Composition and structure of Fe(III)-precipitates formed by Fe(II) oxidation in water at near-neutral pH: interdependent effects of phosphate, silicate and Ca. Geochem. Cosmochim. Acta 162, 220–246.
Si, Y., Li, G., Zhang, F., 2017. Energy-efficient oxidation and removal of arsenite from groundwater using air-cathode iron electrocoagulation. Environ. Sci. Technol. Lett. 4 (2), 71–75.
Strugholtz, S., Sundaramoorthy, K., Panglisch, S., Lerch, A., Brügger, A., Gimbel, R., 2005. Evaluation of the performance of different chemicals for cleaning capillary membranes. Desalination 179 (1), 191–202.
Timmes, T.C., Kim, H.-C., Dempsey, B.A., 2010. Electrocoagulation pretreatment of seawater prior to ultrafiltration: pilot-scale applications for military water purification systems. Desalination 250 (1), 6–13.
van Genuchten, C.M., Bandaru, S.R., Surorova, E., Amrose, S.E., Gadgil, A.J., Pena, J., 2016. Formation of macroscopic surface layers on Fe(0) electrocoagulation electrodes during an extended field trial of arsenic treatment. Chemosphere 153, 270–279.
van Genuchten, C.M., Dalby, K.N., Ceccato, M., Stipp, S.L.S., Dideriksen, K., 2017. Factors affecting the Faradaic efficiency of Fe(0) electrocoagulation. Journal of Environmental Chemical Engineering 5 (5), 4958–4968.
van Genuchten, C.M., Peña, J., Amrose, S.E., Gadgil, A.J., 2014. Structure of Fe (III) precipitates generated by the electrolytic dissolution of Fe (0) in the presence of groundwater ions. Geochem. Cosmochim. Acta 127, 285–304.
Voegelin, A., Senn, A., Kaegi, R., Hug, S., Mangold, S., 2013. Dynamic Fe-precipitate formation induced by Fe(II) oxidation in aerated phosphate-containing water. Geochem. Cosmochim. Acta 117, 216–231.
Wan, W., Pepping, T., Banerji, T., Chaudhari, S., Giammar, D., 2011. Effects of water chemistry on arsenic removal from drinking water by electrocoagulation. Water Res. 45 (1), 384–392.
Xie, S., Yuan, S., Liao, P., Tong, M., Gan, Y., Wang, Y., 2017. Iron-anode enhanced sand filter for arsenic removal from tube well water. Environ. Sci. Technol. 51 (2), 889–896.